### Tanzania Journal of Science

Volume 51(3), 2025





# Dynamic LQR control for improved DC link voltage stability in grid-integrated solar PV system

Mwanajuma Gora<sup>1</sup>, Peter Makolo<sup>1†</sup>, Francis Mwasilu<sup>1</sup> and Jackson J Justo<sup>1,2</sup>

<sup>1</sup>Department of Electrical Engineering, University of Dar es Salaam, P. O. Box 35091, Dar es Salaam, Tanzania; <sup>2</sup>Faculty of Control Systems and Robotics, ITMO University, St. Petersburg, Russia

### Kevwords

Dynamic converter control; LQR method; SMC method' Gridintegrated solar PV; DC voltage stability

### Abstract

The integration of photovoltaic (PV) systems into power grids poses a significant challenge to voltage stability, especially at the DC link. Fluctuations in solar irradiance directly cause power variations and instability in this critical interface. If not properly controlled, this variability can lead to inefficiencies, equipment damage, and widespread grid disturbances. To address the abovementioned challenge, this paper proposes a dynamic converter control strategy designed to enhance DC link voltage stability in grid-integrated solar PV system. The core of the proposed control system is based on a Linear Quadratic Regulator (LQR) mechanism, implemented within a two-stage, PV grid connected system with LCL-filtered three three-phase voltage source converter (VSC). Unlike conventional methods such as Sliding Mode Control (SMC), which can suffer from chattering effects, the proposed LQR approach enhances the performance of grid connected solar PV systems. The proposed scheme allows the designed LQR technique to dynamically and optimally adjust its control parameters in response to fluctuating PV power generation, thereby maintaining optimal voltage stability. Simulation results demonstrate that the LQR control system effectively mitigates DC-link voltage fluctuations. Furthermore, compared to the conventional SMC method, the proposed LQR approach significantly enhances the overall system's robustness and reliability

### Introduction

Renewable energy has become a mature and reliable source of power generation, with solar photovoltaic (PV) systems emerging as one of the most promising technologies due to their pollution-free nature and global availability (Johnson et al. 2020, Tambunan et al. 2020). Over the past two decades, PV power plants have experienced significant growth in generation and grid integration (Masenge & Mwasilu 2020). Generally, renewable energy sources (RES), such as geothermal, biomass, hydro, tidal, wind, and solar, play a critical role in electricity generation, driven by environmental concerns

and the need for energy security (Energy. 2016, Kroposki et al. 2017). Among these, solar energy holds the highest global potential due to its widespread availability. Solar technologies are categorized into two main types: solar PV, which converts sunlight directly into electricity using semiconductor materials, and solar thermal, which uses concentrated solar power (CSP) to generate heat energy (Mathiesen et al. 2011, Mkoi et al. 2025).

Despite the advantages of solar PV systems, their high penetration levels pose significant challenges in maintaining grid stability, particularly at the DC link voltage, which

Received 28 May 2025; Revised 17 Sep 2025; Accepted 19 October 2025; Published 30 October 2025 https://doi.org/10.65085/2507-7961.1060

© College of Natural and Applied Sciences, University of Dar es Salaam, 2025 ISSN 0856-1761, e-ISSN 2507-7961

Torresponding Author: makolo.peter@gmail.com

interfaces the PV array output and inverter input (Monti et al. 2020, Nouti et al. 2021). Recent developments in PV control systems include Active Disturbance Rejection Control (ADRC), Model Predictive Control (MPC), machine learning-based forecasting/control approaches (Zhou et al. 2021, Pannell et al. 2013, Makolo et al. 2021). ADRC offers robustness against disturbances but requires complex tuning, while machine learning methods demand extensive training data, limiting applicability in resource-constrained systems. MPC provides predictive capabilities but incurs high computational overhead (Gursov et al. 2021). In contrast, the proposed LQRbased approach balances simplicity and performance, dynamically adapting irradiance variations without greater efforts in manual retuning. Conventional Sliding Mode Control (SMC) suffers from chattering, overshoot, and prolonged settling times, which degrade system performance under rapid irradiance changes (Pannell et al. 2013, Mohammed et al. 2019). Precise control of the time-varying DC link voltage is thus essential for reliable PV system operation.

Further studies, such as (Imtiaz et al. 2025), highlight the challenges introduced by the stochastic nature of renewable energy sources, particularly solar power. These inherent fluctuations in PV generation can lead to DC link voltage instability, resulting in reduced efficiency, system failures, and potential equipment damage (Justo et al. 2025, Krismanto et al. 2018, Makolo et al. 2025). While various control strategies exist for PV systems, many conventional methods fail to effectively respond to rapid variations in irradiance (Justo et al. 2025, Murillo-Yarce et al. 2020). For instance, traditional Sliding Mode Control (SMC) suffers from significant drawbacks, including overshoot, prolonged settling times, and instability caused by chattering effects. Chattering, characterized by high-frequency oscillations in the control signal, can lead to increased wear on components and degrade overall system performance (Ali & Arbos 2020). These limitations severely impact control precision,

particularly during sudden irradiance changes (Ordóñez & Ríos 2013).

To address these challenges, this study introduces a Linear Quadratic Regulator (LQR) control strategy for enhancing DC link voltage stability in PV-integrated grids under varying irradiance conditions (Zhou et al. 2021). A key advantage of this method lies in its inherent robustness, which allows it to maintain system stability despite significant irradiance fluctuations. Unlike conventional controllers that often necessitate manual retuning under changing conditions, the proposed LQR-based control ensures consistent performance without additional parameter adjustments, thereby improving system resilience and operational efficiency (Kim et al. 2014). This approach inherently avoids the chattering effects associated with SMC and enhances transient response and overall voltage regulation during rapid irradiance fluctuations. By implementing this advanced control strategy, PV systems can achieve improved voltage stability, higher power quality, and increased operational reliability (Kumar & Jerome 2016).

### **Novel Contributions**

proposed LQR control strategy introduces a novel application tailored for two-stage PV system integrated in the grid network through an LCL-filtered, three-phase voltage source converters (VSCs). Unlike the prior LQR implementations, which often rely on static parameter settings, the proposed approach incorporates an LQR design that dynamically adjusts control parameters to mitigate rapid irradiance fluctuations. This control strategy enhances DC link voltage stability under varying solar irradiance conditions, addressing a critical challenge in grid PV integrated into network. Additionally, the proposed LQR avoids chattering effects inherent in SMC, as demonstrated in the simulation results Section, offering superior transient response and robustness.

### **Solar PV Array Modeling**

Solar Photovoltaic (PV) technology is considered one of the most promising

renewable energy sources due to its ability to generate electricity without causing environmental pollution (Villalva et al. 2009). The fundamental equations for modeling a solar PV array are presented in (1) to (3) (Villalva at al. 2009). However, the basic PV cell equation, as expressed in (1), does not fully represent the practical I–V characteristics of a PV array, which typically

consists of numerous interconnected PV cells. To accurately capture the electrical behavior at the terminals of the PV array, additional parameters must be incorporated into the fundamental equation, as demonstrated in (2). The enhanced equivalent circuit, which accounts for these parameters, is shown in Fig. 1 (Masenge & Mwasilu 2020, Tambunan et al. 2020).

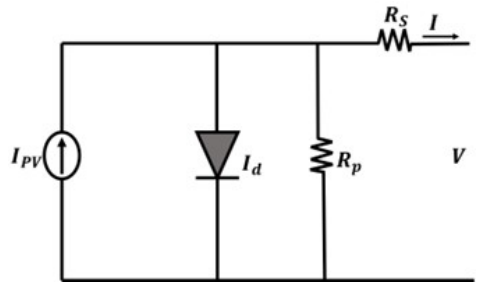


Figure 1: Circuit model for PV panel

$$I_d = I_{0,cell} \left[ \exp \left( \frac{qV}{akT N_s} \right) - 1 \right]$$
(1)

$$I = I_{pv} - I_0 \left[ \exp \left( \frac{V + I R_s}{V_t a} \right) - 1 \right] - \frac{V + I R_s}{R_p}$$
(2)

where  $I_{pv}$  and  $I_0$  are the PV and saturation currents of the array, respectively.  $R_s$  is the identical series resistance of the array and  $R_p$  is the identical parallel resistance. On the other hand, a is the diode ideality constant, while  $V_t$  is the thermal array voltage which is achieved by applying (3).

$$V_{t} = \frac{N_{s}kT}{q}$$
(3)

From (3),  $N_s$  is the number of series connected cells, k is the Boltzmann constant  $1.3806503 \times 10^{-23}$  J/K, T is the p-n junction temperature (in Kelvin), q is the charge of the electron  $1.60217646 \times 10^{-19}$  |C|.

The current output from the PV cells was calculated using (2), which models the

current-voltage (I-V) characteristics under varying irradiance and temperature conditions. To implement this in practice, the solar PV array was designed using MATLAB/Simulink software based on the system requirements. The module decided was 1Sotech 15TH-215-P with parameters, which are shown in Table 1.

The solar PV system, with a power rating of 100 kW was designed and implemented in this paper. As illustrated in Table 1, the voltage for a single module for maximum

power ( $V_{mp}$  was 29 V. Then by connecting 10 modules in series ( $N_{\rm s}$ , the voltage is calculated as shown in (4).

**Table 1:** Characteristics of PV array

Module data	Value		
Maximum Power, $P_m$	213.15W		
Voltage at the Maximum Power Point, $V_{\it mpp}$	29V		
Current at Maximum Power Point, $I_{mpp}$	7.35A		
Cells per Module, $N_{\it cell}$	60		
Open Circuit Voltage, $\boldsymbol{V}_{oc}$	36.3 V		
Short Circuit Current, $I_{sc}$	7.84 A		
Temp. Coefficient of $V_{\mathit{oc}}$	0.36099%/oC		
Temp. coefficient of $I_{\mathrm{sc}}$	0.102%/oC		

$$V = V_{mp} \times N_s$$
(4)

Then, the voltage calculated in (4) is substituted in (5) to obtain the total current given the system power of 100kW.

$$I = \frac{P}{V}$$
(5)

Since the current for a single module at maximum power ( $I_{mp}$  was  $7.35\,A$  as shown in Table 1. Then, the number of parallel connected module strings is determined using (6).

$$N_p = \frac{I}{I_{mp}}$$
(6)

### **Boost Converter Design**

The boost converter's input voltage corresponds to the PV array's maximum power point (MPP) voltage ( $V_{pv}$ ), set at 290 V as derived from (1). The associated circuit configuration is illustrated in Fig. 2 (Viswambaran et al. 2016).

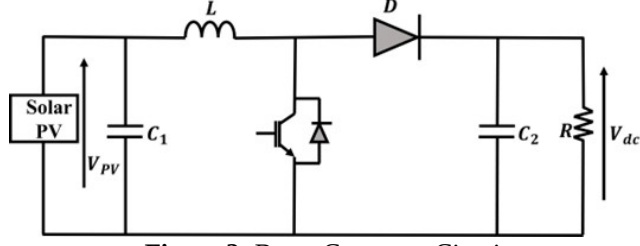


Figure 2: Boost Converter Circuit

The boost converter's inductor (L) was sized giving to the duty cycle determined by (7).

$$D = \frac{V_{dc} - V_{pv}}{V_{dc}}$$

The calculated value of the boost inductor (L) was given by the (8) (Motahhir et al. 2018).

$$L = \frac{V_{mp} \times D}{\Delta i_{rp} \times f_{s}}$$
(8)

where  $\Delta i_{rp}$  is ripple current, which was considered as 6% of the MPP solar PV current and  $f_s$  is switching frequency.

The input capacitor was designed to suppress voltage ripple limited to  $1\% \Delta V$  and ensure stable current delivery to the inductor, as calculated using (9) (Motahhir et al. 2018). This follows established principles for minimising PV-side fluctuations (Masenge & Mwasilu 2020).

$$C_1 = \frac{D}{8 \times f_s \times L \times \Delta V}$$

$$(9)$$

The DC bus capacitor was calculated based on a DC bus voltage of 600 V, as obtainable in (10).

$$C_2 = \frac{P_{dc}}{\omega \times V_{dc} \times \Delta V_{dc}}$$

$$(10)$$

### **Proposed Control Strategy**

This section outlines the system configuration analysed in this study, as illustrated in Fig. 3. The configuration is a two-stage, three-phase grid-connected solar PV. It comprises a solar PV array that delivers power to the grid via a DC-DC boost converter, followed by a voltage source converter (VSC) and an LCL filter. Then, there is a need to measure the grid current and

voltage synchronized by the PLL, and the information is sent to the inverter control. Also, to obtain the source voltage from the DC link, which is used as an input of the inverter control. By using the proposed LQR control method, the inverter control algorithm generates a switching signal to control the VSC, which also controls the voltage and current and maintains the stability of the DC link voltage.

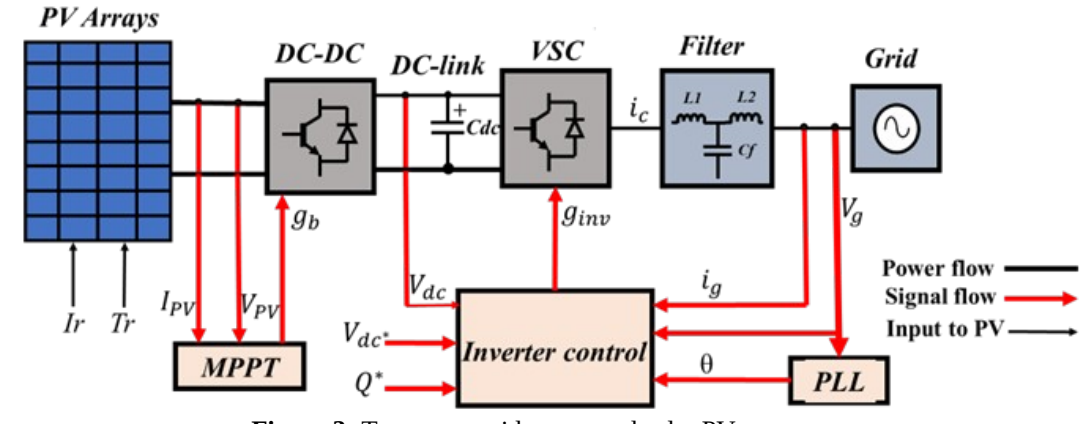


Figure 3: Two-stage grid-connected solar PV system

### Solar PV LCL Modelling

When considering the LCL filter, the circuit dynamics in the *abc* reference frame is as shown in (11).

$$\begin{cases} u = R_1 i_c + L_1 \frac{di_c}{d} + u_c \\ u_c = R_2 i_g + L_2 \frac{di_g}{d} + u_g \\ C_f \frac{du_c}{dt} = i_c - i_g \end{cases}$$

$$(11)$$

There are three state variables for each phase: the capacitor voltage  $u_c$ , the converter's current  $i_c$  and the grid current  $i_g$ . The dynamics of the converter side and grid side voltages and currents can be represented using space phasor as depicted in in (12) (Kumare & Jerome 2016).

$$\begin{split} \vec{u}(t) &= R_1 \vec{i}_c(t) + L_1 \vec{i}_c(t) + j \omega L_1 \vec{i}_c(t) + \vec{u}_c(t) \\ \vec{u}_c(t) &= R_2 \vec{i}_g(t) + L_2 \vec{i}_g(t) + j \omega L_2 \vec{i}_g(t) + \vec{u}_g(t) \\ \vec{i}_c(t) &= \vec{i}_g(t) + j \omega C_f \vec{u}_c(t) + C_f \vec{u}_c(t) \end{split}$$

The LCL filter system comprises key electrical quantities represented as vectors in the time domain: the converter-side voltage  $\vec{u}_c(t)$ , the filter capacitor voltage  $\vec{u}_c(t)$ , and the grid voltage  $\vec{u}_g(t)$  measured at the point of common coupling (PCC). Additionally, the converter-side current  $\vec{i}_c(t)$  and the grid side current  $\vec{i}_g(t)$  define the current flow through the filter. The filter parameters include the converter-side inductance  $L_1$  with its internal

resistance  $R_1$ , the grid-side inductance  $L_2$ with resistance  $R_2$ , and capacitance  $C_f$ . The grid operates fundamental frequency  $\omega$ . To simplify analysis and control design, the system equations transformed are into the synchronous *dq*-axis reference frame. This transformation, followed by algebraic rearrangement, yields a state-space model as in (13).

$$\vec{\dot{x}}(t) = A\vec{\dot{x}}(t) + B\vec{\dot{u}}(t) + B_w\vec{\dot{u}}_g(t)$$

$$\vec{\dot{y}}(t) = C\vec{\dot{x}}(t)$$
(13)

where:

$$\vec{x}(t) = \begin{bmatrix} \vec{i}_{cd}(t) & \vec{i}_{cq}(t) & \vec{i}_{gd}(t) & \vec{i}_{gq}(t) & \vec{u}_{cd}(t) & \vec{u}_{cq}(t) \end{bmatrix}^{T} \\ \vec{y}(t) = \begin{bmatrix} \vec{i}_{cd}(t) & \vec{i}_{cq}(t) \end{bmatrix}^{T}$$
(14)

$$A = \begin{bmatrix} -R_1 & \omega & 0 & 0 & \frac{-1}{L_1} & 0 \\ -R_1 & -R_1 & 0 & 0 & \frac{-1}{L_1} & 0 \\ -\omega & \frac{-1}{L_1} & \frac{-R_2}{L_2} & \omega & 0 & \frac{-1}{L_1} \\ 0 & 0 & \frac{-1}{L_2} & \frac{-R_2}{L_2} & \frac{-1}{L_2} & 0 \\ 0 & 0 & -\omega & \frac{1}{L_2} & \frac{-1}{L_2} & \omega \\ \frac{1}{C_f} & \frac{1}{C_f} & \frac{-1}{C_f} & 0 & 0 \\ 0 & \frac{1}{C_f} & 0 & \frac{-1}{C_f} & -\omega \end{bmatrix}$$

$$B = \begin{bmatrix} \frac{1}{L_1} & 0 \\ 0 & \frac{1}{L_1} \\ 0 & 0 \\ 0 & 0 \\ 0 & 0 \\ 0 & 0 \end{bmatrix} \qquad B_w = \begin{bmatrix} 0 & 0 \\ 0 & 0 \\ \frac{1}{L_2} & \frac{1}{L_2} \\ 0 & 0 \\ 0 & 0 \end{bmatrix} \qquad C = \begin{bmatrix} 0 & 0 \\ 0 & 0 \\ 1 & 0 \\ 0 & 1 \\ 0 & 0 \\ 0 & 0 \end{bmatrix}^T$$

### **Proposed LQR Control Method**

The LQR is an optimal control method that stabilizes dynamic systems while minimizing a cost function. This cost function balances two key objectives: maintaining system performance (keeping the state close to the desired setpoint) and minimizing control effort. LQR operates within a state-space basis, where it calculates an optimal feedback gain matrix. This matrix ensures system stability, efficiently drives the system toward its target state, and optimizes control input usage. Due to its robustness, LQR is especially effective for linear time-invariant (LTI) systems as represented in (13) (Kim et al. 2014).

An LQR to find the optimal control law that minimizes a cost function (15), ensuring system stability and performance while penalizing both deviations from the desired state and control effort.

$$J = \int_{0}^{\infty} \left( x ||T||(t) Q_{x}(t) + u^{T}(t) R_{u}(t) \right) dt (15)$$

Q is a positive semi-definite matrix that penalizes deviations from the desired state. R is a positive definite matrix that penalizes the control effort. The performance of an LQR

controller depends on the proper selection of the Q and R matrices in the cost function (Kim et al. 2015) . The diagonal matrices Q and R are defined as:  $Q = diag(q_1, q_2, \ldots, q_6)$  and  $R = diag(r_1, r_2)$ .

Deriving the optimal control law involves first expressing the cost function in a quadratic form. By completing the square, the optimal control input can be isolated. The optimal steps from (16) to (22). (Kim et al. 2014; control law is then determined by following Kumar & Jerome 2016).

$$J = x_o^T P x_o - x_o^T P x_o + \int_0^\infty \left( x^T || Q_x + u^T R_u \right) dt$$
 (16)

$$J = x_o^T P x_o + \int_0^\infty \left( \frac{d}{dt} (x || T P x) + x^T Q_x + u^T R_u \right) dt$$
(17)

Equation (17), is further expanded as depicted in (18) and (19).

$$\frac{d}{dt}(x||TPx) = \dot{x}^T P x + x^T P \dot{x} = (Ax + Bu)^T P x + x^T P (Ax + Bu)$$
(18)

$$J = x_o^T P x_o + \int_0^\infty \left( x^T \left( A^T P + PA + Q \right) x + u^T R_u \right) \left| + x^T PB u + u^T B^T P x \right| dt$$

$$u^{T} R_{u} + x^{T} PBu + u^{T} B^{T} Px = (u + R^{-1} B^{T} Px)^{T} R(u + R^{-1} B^{T} Px) - x^{T} (PBR^{-1} B^{T} P) x$$
(19)

By replacing  $u = -R^{-1}B^T P_X$  in (19), (20) is obtained.

$$J = x_o^T P x_o + \int_0^\infty \left[ x^T (A^T P + PA + Q - PB R^{-1} | |B^T P) x + (u + R^{-1} B^T Px)^T R (u + R^{-1} B^T Px) \right] dt$$
(20)

Equation (20) is further simplified into (21).

$$A^{T} P + PA + Q - PB R^{-1} B^{T} P = 0 (21)$$

The equation (21) is known as the Algebraic Riccati Equation (ARE). It is a matrix quadratic equation that can be solved for the auxiliary matrix P given (A, B, Q, R). Once P is found, the optimal feedback gain matrix (K) is computed in (22).

$$K = R^{-1} B^T P \tag{22}$$

The optimal controller can be designed by (23), which is called the optimal control law.

$$u(t) = -Kx(t)$$
(23)

where K is the optimal feedback gain matrix (Kumare & Jerome 2016), which yields a closed-loop system. Using this K from the control law, the state space of the system becomes as depicted in (24).

$$\dot{x} = (A - BK)x + Bv = A_c x + B_w u_g$$

$$A_c = (A - BK)$$
(24)

This procedure can be executed in MATLAB using the lqr(A,B,Q,R) function. Fig. 4 summarizes the LQR method for a system with various parameters as shown in the figure.

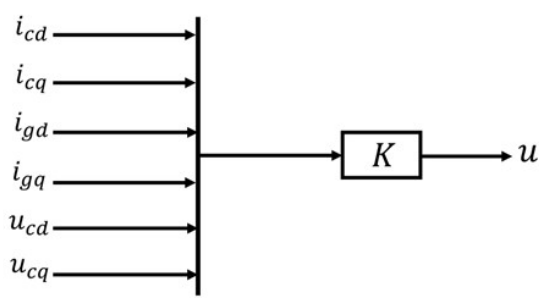


Figure 4: Block diagram of the LQR method

### **System Controllability and Observability**

The LOR design relies on the system being controllable and observable. For the statespace model in (13), we verify these properties using the controllability and observability matrices. The controllability matrix is defined  $C = \begin{bmatrix} BABA^2B...A^{n-1}B \end{bmatrix}$  where A and B are the system and input matrices from (13), and n represents the dimension of the system. Similarly, the system is controllable if *C* has full rank, i.e., rank(C) = n. Similarly, the observability matrix is  $O = \begin{bmatrix} C^T A^T C^T \dots A^{n-1} C^T \end{bmatrix}$  where *C* is the output matrix. The system is observable if rank(O) = n, where *n* is the dimension of the system. Numerical evaluation confirms that both matrices C and O have full rank, satisfying the LQR requirements. It should be **Table 2:** System parameter for modelling

noted that the LTI system in (13) is widely used in LCL-based converter control design in the literature. It is known that observability is the possibility to reconstruct the full 'signal' of the system from the data obtained from the input and output measurements. In this paper it is assumed that all the signal are available through sensors.

#### **Results and Discussion**

System parameters, including voltage, current, and rated power, are critical for designing and analysing grid-connected PV systems. These values are essential for designing, analysing, and controlling systems to ensure they operate safely, efficiently. Table 2 presents system parameters used to validate the performance of the proposed method.

Parameters	Value
System Frequency	f = 50 Hz
Line to Line Voltage	$V_{a}=400V$
DC Link Voltage	$V_{dc} = 600 V$
DC Link Capacitor	$C_{dc} = 35.378  mF$
Converter-Side Inductor	$L_1 = 500  \mu H$
Grid-Side Inductor	$L_2 = 500  \mu H$
Filter Capacitor	$C_f = 100  \mu F$
Switching Frequency	$f_s = 10  kH$

To facilitate a comparative analysis between the LQR and SMC controllers, Table 3 presents the key parameters governing the SMC system.

Table 3: Sliding Mode Control (SMC) Parameters

Parameters	Value
Sliding Surface Gain ( <i>ks</i> )	0.5
Boundary Layer Thickness $(\phi)$	0.02
Switching Frequency ( <i>f</i> <sub>s</sub> )	10 kHz
Hysteresis Band	0.01 V

### **Simulation Results**

In LQR design, the gain matrix K is calculated using MATLAB's lqr(A, B, Q, R)command, where Q and R are weighting matrices determining the trade-off between state regulation and control effort. The matrix Q, which must be positive semi-definite, assigns penalties to deviations in the system states; higher values in Q place greater importance on minimising state errors, leading to quicker convergence and improved dynamic response. This change effectively shifts the closed-loop poles further into the left of the s-plane, increasing system damping and speeding up the decay of transients. On the other hand, R, which must be positive definite, penalises excessive control input. By carefully tuning Q and R, it can strike a balance between rapid state regulation and

control usage. Increasing efficient generally results in a more aggressive response (Kumare & Jerome, 2016). The LQR framework guarantees stability as long as (A, B) is controllable and the weighting matrices satisfy the required definiteness. conditions. The selection of weighting matrices *Q* and *R* in the LQR design is guided by the closed-loop system dynamics (A - BK), which determines the pole placement. As illustrated in Fig. 5, variations in the *Q* matrix directly influence the of the closed-loop movement representing how different weightings affect the system's dynamic response and stability characteristics. This relationship enables systematic tuning of the controller by adjusting *O* to achieve desired pole locations that meet performance specifications.

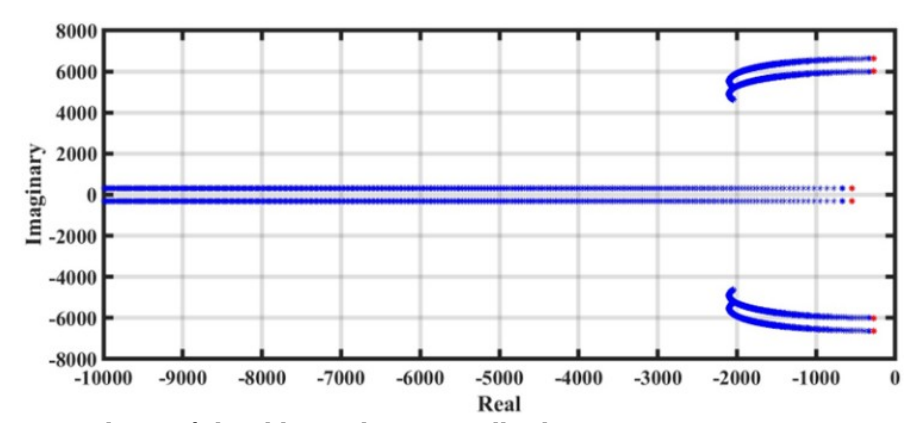


**Figure 5:** Evolution of closed-loop poles in controller design

The proposed system's performance is evaluated across multiple operational scenarios, as outlined in the following subsections:

# Condition 1: Constant Irradiance with LQR method

The photovoltaic system was evaluated under stable environmental conditions with a

constant irradiance of  $1000~W/m^2$  and a constant temperature of  $25^{\circ}C$  to evaluate its operational performance. As demonstrated in Fig. 6, the DC-link voltage regulator demonstrated excellent stability control by precisely maintaining the output voltage at the target 600~V throughout the test. The invariant test conditions ensured consistent DC power generation without any

fluctuations, as both the solar irradiance and panel temperature remained steady. This controlled environment effectively eliminated potential voltage instabilities that typically arise from variable solar power, allowing the system to operate with optimal reliability. The results confirm the voltage regulator's capability to deliver stable performance under constant conditions.

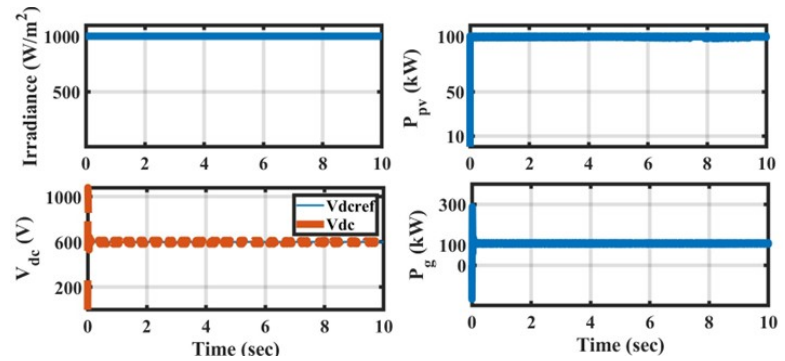
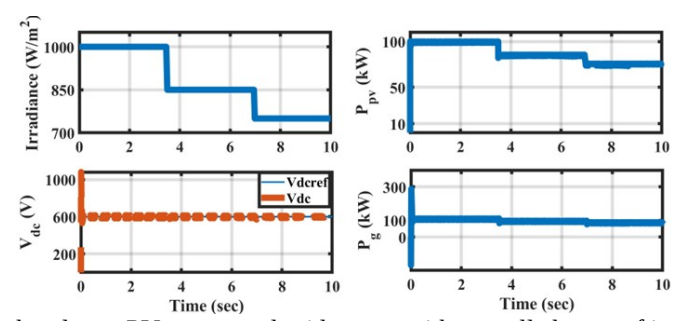


Figure 6: DC link voltage, PV power and grid power with constant irradiance

## (i) Scenario 1: Small Change (≤ 15%) of Irradiance with Sliding Mode Control

The MATLAB/Simulink model of the PV integrated system was tested under small irradiance variations at a fixed temperature of 25°C. Employing the conventional SMC for regulation. As shown in Fig. 7, the system initially operated at 1000 W/m², maintaining a stable DC-link voltage of 600 V, confirming control performance. When irradiance dropped to 850 W/m² (3.5–7 s), the PV output power and grid-injected power decreased proportionally, yet the DC link

voltage remained steady, demonstrating the controller's ability to compensate for reduced solar generation. A further decline to 750 W/m² (7–10 s) introduced only minor voltage fluctuations, well within permissible limits. The SMC effectively suppressed disturbances, dynamically adjusting control parameters to sustain stability despite irradiance changes. These findings validate the robustness of the SMC in real-world conditions, ensuring reliable grid integration of the PV system.



**Figure 7:** DC link voltage, PV power and grid power with a small change of irradiance

# (ii) Scenario 2: Large Change (15% - 50%) of Irradiance with Sliding Mode Control

The presentation of the grid-connected solar photovoltaic (PV) system was evaluated under varying solar irradiance conditions while maintaining a constant temperature,

using a conventional SMC for system regulation. As illustrated in Fig. 8, when irradiance drops from  $1000~W/m^2$  to  $500~W/m^2$  and further to  $100~W/m^2$ , the SMC struggles to maintain the DC link voltage at its reference value, resulting in significant

fluctuations and instability in the injected grid power. This inadequate voltage regulation under rapidly changing irradiance conditions not only diminishes system efficiency but also compromises the reliability of power transfer to the grid. The conventional SMC's inability to quickly adapt to abrupt environmental changes leads to a sluggish dynamic response, causing long deviations from the desired operating point. Consequently, power quality deteriorates, posing challenges for grid stability and potentially violating grid

compliance standards. Further analysis, as shown in Fig. 9, indicates that although the grid voltage remains stable throughout these irradiance variations, the grid current and the dq-axis reference currents key parameters for controlling active and reactive power flow exhibit noticeable oscillations. These oscillations reflect the dynamic mismatch between the controller's reference commands and the actual system response, decline the smooth operation of the inverter and potentially affecting power quality.

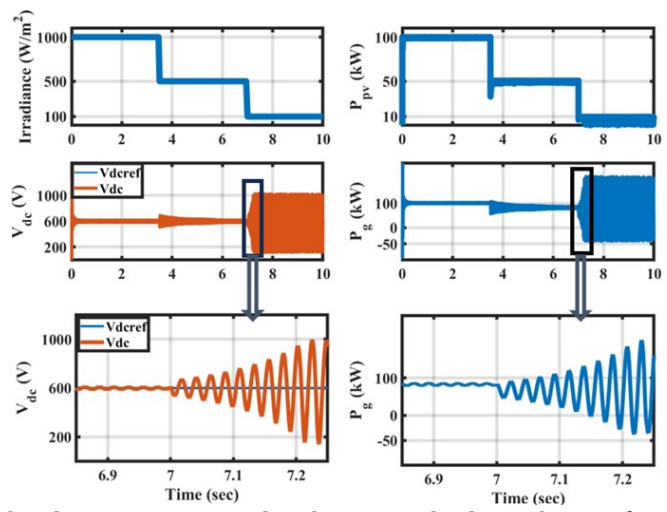


**Figure 8:** DC link voltage, PV power and grid power with a large change of irradiance

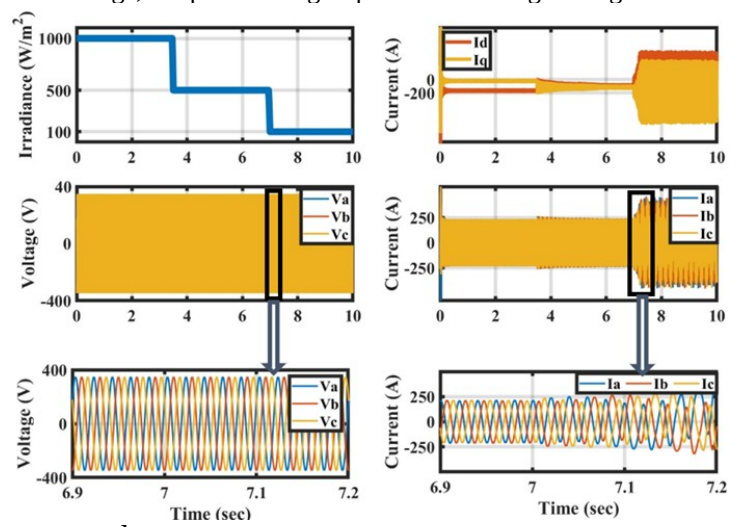


**Figure 9:** Grid current, *dq* current and grid voltage with a large change of irradiance

### (iii) Scenario 2: Large Change (15% - 50%) of Irradiance with Linear Quadratic Regulator

Figure 10 establishes the performance of Flexible converter control, which is the LQR controller in maintaining the DC-link voltage at a stable 600 V under standard irradiance conditions (1000 W/m<sup>2</sup>) for the initial 3.5 s. Even as the irradiance decreases between 3.5 s and 7 s, the controller continues to regulate the voltage with minimal deviation, showcasing its robustness against environmental variations. This stability is achieved through the carefully optimised Q matrix and exactly calculated feedback gains. enabling the LQR to adapt to changing conditions. The controller's ability to maintain voltage regulation highlights its effectiveness in preserving system stability, even during sudden shifts in solar input. Further validating its performance, Fig. 11 confirms that the LQR controller successfully stabilises both the grid current and *dq*-axis reference currents despite irradiance fluctuations. Notably, the grid voltage remains steady, demonstrating the controller's capability to decouple voltage current regulation effectively. ensures smooth power injection into the grid. The consistent performance across varying operating conditions highlights the LQR controller's dvnamic adaptability reliability, making it a robust solution for grid-connected PV systems under variable irradiance scenarios.

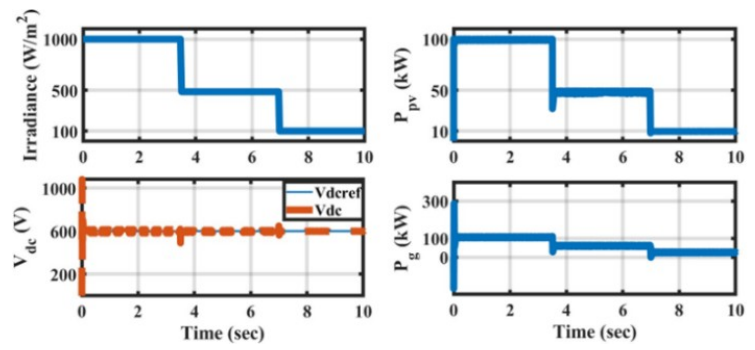


**Figure 10:** DC link voltage, PV power and grid power with a large change of irradiance

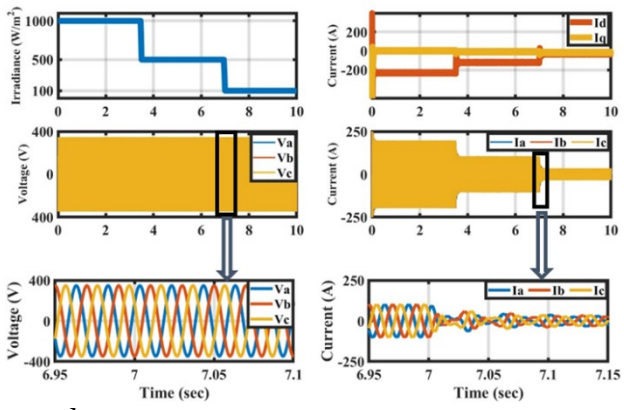


**Figure 11:** Grid current, dq current and grid voltage with a large change of irradiance

# (i) Scenario 3: Quick Change of Irradiance with Sliding Mode Control

The simulation results in Fig. 12 demonstrate the challenges faced by the conventional SMC in handling rapid and continuous solar irradiance variations.

Although the SMC effectively regulates the DC-link voltage at 600 V under steady-state conditions, its performance deteriorates significantly during dynamic irradiance changes, leading to fluctuations in PV power output. This instability generates in the DC-

link voltage, causing deviations from the reference value and resulting in unreliable grid power injection. The inability of the SMC to mitigate these oscillations highlights its limited adaptability under transient conditions, ultimately compromising the system's power quality and reliability. As depicted in Fig. 13, these instabilities are further clear in the grid current and dq-axis reference currents, which exhibit undesirable oscillations despite the grid voltage remaining stable. These fluctuations indicate a dynamic mismatch between the controller's response

and the actual system behavior, reducing the inverter's ability to maintain consistent active and reactive power delivery. The determined instability in critical control variables suggests that the conventional SMC, while robust in steady-state operation, lacks the necessary flexibility to ensure full system stability under rapidly changing environmental conditions. This highlights the need for more adaptive control strategies, such as flexible converter control, to enhance dynamic performance and ensure reliable power injection into the grid.

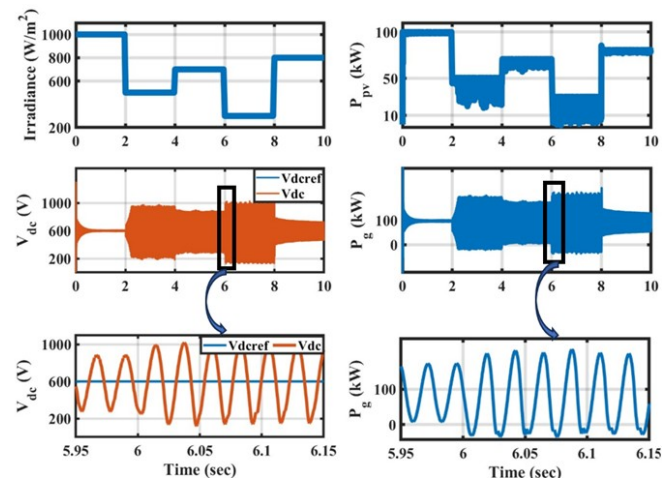
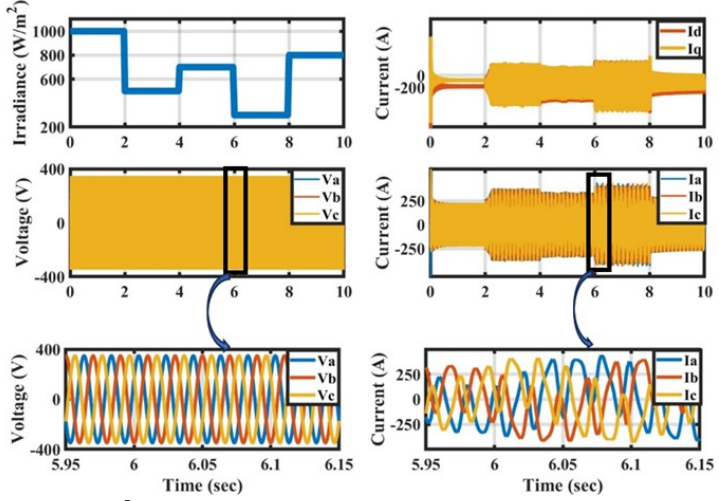


Figure 12: DC link voltage, PV power and grid power with quick change of irradiance



**Figure 13:** Grid current, *dq* current and grid voltage with a quick change of irradiance

### (iv) Scenario 3: Quick Change of Irradiance with Linear Quadratic Regulator

As shown in Fig. 14, a sudden and rapid change in solar irradiance causes significant

fluctuations in the output power from solar These fluctuations directly system. influence the DC-link voltage, leading to instability in the power transferred to the grid. However, the implementation of a LQR plays a crucial role in maintaining system stability. The LQR dynamically adjusts the control inputs to minimise the variation of the DClink voltage from its reference value, thereby ensuring consistent performance even in the presence of rapid irradiance changes. Meanwhile, Fig. 15 illustrates the response of grid-side variables under identical irradiance variations. While the grid voltage remains

demonstrating steady. effective voltage regulation, the grid current and corresponding *dq*-axis reference currents adjust in response to the fluctuating solar input. These variations are natural, reflecting the system's adaptation to changing power generation. Despite these dynamics, the LQR controller maintains robust performance. effectively suppressing the effects irradiance variability. By ensuring smooth and synchronised current injection into the grid, the LQR enhances the reliability of gridconnected PV systems under environmental conditions.

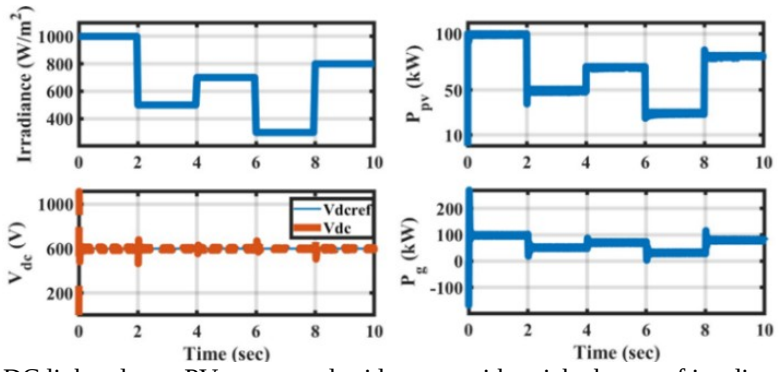
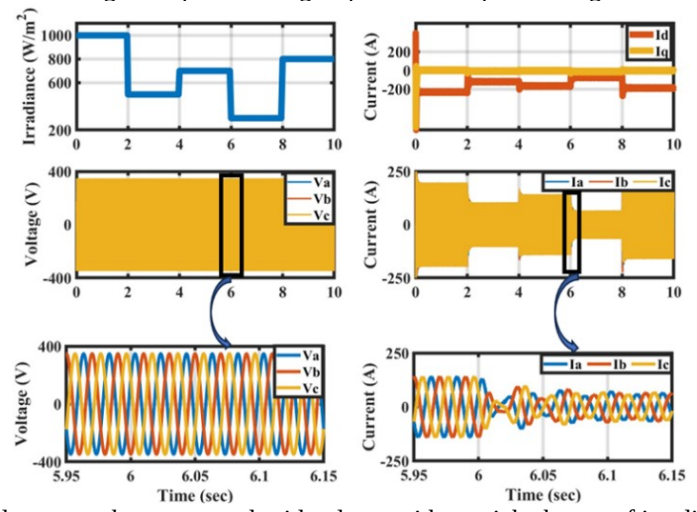


Figure 14: DC link voltage, PV power and grid power with quick change of irradiance



**Figure 15:** Grid current, *dq* current and grid voltage with a quick change of irradiance

### **Performance Metrics Table**

Table 4 is presented to analyse and compare between the proposed adaptive LQR method with SMC on different performance metrics. The LQR controller under nonlinear conditions maintains the DC link voltage within 1% of the 600 V reference, with a settling time of 0.019 s and RMSE of 0.4 V. In contrast, the SMC exhibits larger deviations (RMSE = 1.8 V) and a longer

settling time (0.07 s). These results confirm the LQR's robustness against load and

temperature variations, complementing its performance under irradiance changes.

Table 4: Performance Metrics for LQR and SMC Controllers

Scenario	Control	THD	Settling	RMSE (V)
	Approach	(%)	Time (s)	
Constant	LQR	8.0	0.015	0.3
Irradiance	SMC	2.5	0.05	1.2
Small	LQR	1.0	0.018	0.4
Irradiance Change	SMC	3.0	0.06	1.5
Large	LQR	1.2	0.02	0.5
Irradiance Change	SMC	3.8	80.0	2.1
Quick	LQR	1.3	0.02	0.5
Irradiance Change	SMC	4.2	0.09	2.3
Load/	LQR	1.1	0.019	0.4
Temperature Change	SMC	3.5	0.07	1.8

### Sensitivity Analysis of Q and R Matrices

The performance of the LQR controller depends on the weighting matrices Q and R. To assess sensitivity, we varied O (state penalty) and R (control effort penalty) by ±20% from their nominal values. For Q = diag(10, 10, 1, 1) increasing Q by 20% reduces settling time to 0.015 s but increases control effort by 10%, while decreasing Q increases settling time to 0.025 s. Similarly, varying R from 0.1 to 0.12 or 0.08 adjusts the trade-off between response speed and control input. Results illustrate the DC link voltage response under these variations, confirming that the LQR remains stable with RMSE below 0.6 V across all cases. This analysis validates the robustness of the chosen *Q* and *R* values.

### **Grid Compliance Analysis**

The outdoor PV arrays experience variations irradiance and temperature, which introduce dynamics in the PV output parameters. These variations be must accounted for during control Furthermore, harmonics limits have been set by different standards such as IEEE 1547, IEEE 929, IEC 61727 or Rule 21; and PV plants operators are obliged to adhere to these

limits at the point of coupling (PCC) (Kouro et al. 2015, Panigrahi et al. 2020). To ensure compatibility with grid standards, the LQR controller was evaluated against IEEE 1547 requirements for voltage regulation and power quality. Under all simulation scenarios (constant, small, large, and quick irradiance changes), the LQR maintains THD below 5% (e.g., 1.3% for quick changes, Table 4) and ensures stable grid power injection within acceptable voltage limits (600 V  $\pm$  2%). These results comply with IEEE 1547 and align with EN 50549 standards for European grids, confirming the controller's suitability for practical grid integration.

### Discussion

The LQR control method demonstrates greater performance in stabilizing DC link voltage for grid-integrated photovoltaic (PV) systems compared to conventional SMC techniques. By optimizing a cost function that balances state deviations and control effort, the LQR controller ensures efficient voltage regulation while enhancing dynamic response, a critical advantage in PV systems were rapid power fluctuations due to irradiance variations challenge stability. Simulation results show that the LQR controller effectively suppresses DC link voltage fluctuations, maintaining a

stable voltage profile under steady-state and transient conditions. which often suffer from chattering effects, overshoot, and longer settling times, the LQR approach offers superior damping characteristics and faster transient response. This leads to improved power quality and reliability in grid-tied PV systems, making it a robust solution for mitigating intermittency-related instability.

### Conclusion

This study presents a dynamic Linear Quadratic Regulator (LQR)-based control strategy for stabilizing DC link voltage in grid-connected solar photovoltaic (PV) systems, addressing voltage fluctuations solar irradiance variability. caused by MATLAB/Simulink simulations demonstrate that the LQR helps to maintains the DC link voltage at 600 V with a Total Harmonic Distortion (THD) below 1.3% and a settling time of 0.02 s under rapid irradiance changes, outperforming Sliding Mode Control (SMC) (THD 4.2%, settling time 0.09 s). The controller ensures compliance with IEEE 1547 standards and robustness against load, temperature, and grid transient conditions.

To further validate the proposed LQR controller, hardware-in-the-loop simulation using platforms such as OPAL-RT or dSPACE is a promising future direction. HIL validation would enable real-time testing the controller under realistic grid bridging conditions. the gap simulation and hardware implementation. However, HIL was not pursued in this study due to resource constraints, including the high cost of real-time simulators and the need for specialized hardware interfaces. Future work could leverage HIL to assess the LQR's performance in scenarios involving complex grid dynamics, such as multi-terminal DC grids or islanding conditions, enhancing its applicability to practical PV systems.

Future work includes exploring adaptive tuning algorithms for the LQR's *Q* and *R* matrices and multi-terminal DC grid applications to further enhance grid resilience. This research supports reliable integration of PV systems into smart grids,

reducing dependence on conventional power sources.

### **Conflicts of Interest**

Authors declare that no conflicts of interest. **Acknowledgements** 

The author appreciates the support from the Department of Electrical Engineering, University of Dar es Salaam.

### References

Ali HG and Arbos RV 2020 Chattering free adaptive sliding mode controller for photovoltaic panels with maximum power point tracking. *Energies* 13(21): 5678. https://doi.org/10.3390/en13215678

Gursoy M, Zhuo G, Lozowski AG, and Wang X 2021 Photovoltaic energy conversion systems with sliding mode control. **Energies** 14(19): 6071. https://doi.org/10.3390/en14196071 Viswambaran VK, Ghani A and Zhou E. 2016 Modelling and simulation of maximum power point tracking algorithms & review of MPPT techniques for PV applications. In 2016 5th international conference on electronic devices, systems and applications (ICEDSA) (pp. 1-4). IEEE..

https://doi.org/10.1109/ICEDSA.2016.7818 506

Imtiaz S, Yang L, Munir HM, Memon ZA, Kilic H and Naz MN 2025 DC-link voltage stability enhancement in intermittent microgrids using coordinated reserve energy management strategy. *IET Renew. Power Gener.* 19(1): e13197. https://doi.org/10.1049/rpg2.13197

Johnson SC, Rhodes JD and Webber ME 2020 Understanding the impact of non-synchronous wind and solar generation on grid stability and identifying mitigation pathways. *Appl. Energy*, 262: 114492. https://doi.org/10.1016/j.apenergy.2020.114492

Justo JJ, Demidova G, Lukichev D, Poliakov N, Makolo P and Bansal RC 2025 Synthesis of dynamic virtual-inertia for microgrid system applications. In 2025 International Conference on Intelligent Control, Computing and Communications

- (IC3) (pp. 177–182). IEEE. https://doi.org/10.1109/IC363308.2025.109 57416
- Kim E-K, Mwasilu F, Choi HH and Jung JW 2015 An observer-based optimal voltage control scheme for three-phase UPS systems. *IEEE Trans. Ind. Electron.* 62(4): 2073–2081.

https://doi.org/10.1109/TIE.2014.2351777

- Kouro S, Leon JI, Vinnikov D, Franquelo LG 2015 Grid-connected photovoltaic systems: An overview of recent research and emerging PV converter technology. *IEEE Ind. Electron. Mag.* 9(1): 47-61. https://doi.org/10.1109/MIE.2014.2376976
- Krismanto AU, Mithulananthan N and Krause O 2018 Stability of renewable energy based microgrid in autonomous operation. *Sustain. Energy Grids Netw.*, 13: 134–147.
- https://doi.org/10.1016/j.segan.2017.12.009 Kroposki B, et al. (2017). Achieving a 100% renewable grid: Operating electric power systems with extremely high levels of variable renewable energy. *IEEE Power Energy Mag.* 15(2): 61–73. https://doi.org/10.1109/MPE.2016.2637122
- Kumare V and Jerome J 2016 Algebraic Riccati equation based Q and R matrices selection algorithm for optimal LQR applied to tracking control of 3rd order magnetic levitation system. *Arch. Electr. Eng.*, 65(1): 151–168. https://doi.org/10.1515/aee-2016-0012
- Makolo P, Cheah-Mañe M and Gomis-Bellmunt O 2025 Quantification of virtual inertia from derivative control using a recursive least square with a weighted forgetting method. *Electr. Power Syst. Res.*, 241: 111363.
- https://doi.org/10.1016/j.epsr.2024.111363
  Makolo P, Oladeii I, Zamora R and Lie T-T
  2021 Short-range inertia prediction for
  power networks with penetration of RES. In
  TENCON 2021–2021 IEEE Region 10
  Conference (TENCON) (pp. 765–770).
  https://doi.org/10.1109/TENCON54134.20
  21.9707270
- Masenge IH and Mwasilu F 2020 Modeling and control of solar PV with battery energy

- storage for rural electrification. *Tanz. J. Engrng. Technol.*, 39(1): 47–58.
- Mathiesen BV, Lund H and Karlsson K 2011 100% renewable energy systems, climate mitigation and economic growth. *Appl. Sci.* 88(2): 488–501. https://doi.org/10.1016/j.apenergy.2010.03. 001
- Mkoi P, Makolo PM and Mwasilu FA 2025 Synthetic inertia provision for load frequency control in networks with high penetration of renewable energy sources. *Tanz. J. Eng. Technol.*, 44(1): 245–256.
- Mohamed SR, Jeyanthy PA, Devaraj D, Shwehdi, MH and Aldalbahi A 2019 DC-link voltage control of a grid-connected solar photovoltaic system for fault ridethrough capability enhancement. *Appl. Sci.*, 9(5): 952.

https://doi.org/10.3390/app9050952

- Monti A, Milano F, Bompard E and Guillaud X 2020 *Converter-based dynamics and control of modern power systems*. Academic Press.
- Motahhir S, El Ghzizal A, Sebti S and Derouich A 2018 Modeling of photovoltaic system with modified incremental conductance algorithm for fast changes of irradiance. *Int. J. Photoenergy* 2018: 3286479.

### https://doi.org/10.1155/2018/3286479

- Murillo-Yarce D, et al. (2020). A review of control techniques in photovoltaic systems. *Sustainability*, 12(24): 10598. https://doi.org/10.3390/su122410598
- Nouti D, Ponci F and Monti A 2021 Heterogeneous inertia estimation for power systems with high penetration of converter-interfaced generation. *Energies* 14(16): 5047. https://doi.org/10.3390/en14165047
- Ordóñez CA and Ríos MA 2013 Electromechanical modes identification based on sliding-window data from a widearea monitoring system. Electr. Power Compon. Syst. 41(13): 1264-1279. https://doi.org/10.1080/15325008.2013.816 982
- Panigrahi R, Mishra SK, Srivastava SC, Srivastava AK and Schulz, N. N. (2020). Grid integration of small-scale photovoltaic systems in secondary distribution network

- —A review. *IEEE Trans. Industry Appl.* 56(3): 3178-3195.
- https://doi.org/10.1109/TIA.2020.2979789
- Pannell G, Zahawi B, Atkinson DJ and Missailidis P 2013 Evaluation of the performance of a DC-link brake chopper as a DFIG low-voltage fault-ride-through device. *IEEE Trans. Energy Convers.*, 28(3): 535–542. https://doi.org/10.1109/TEC.2013.2261301
  - https://doi.org/10.1109/TEC.2013.2261301 Energy, B., 2016 Renewables 2017 global status report. Renewable Energy Policy Network for the 21st Century. Paris: REN21.
- Tambunan HB, et al. 2020 The challenges and opportunities of renewable energy source (RES) penetration in Indonesia: Case study of Java-Bali power system. *Energies* 13(22): 5903. https://doi.org/10.3390/en13225903
- Villalva MG, Gazoli JR and Ruppert FE 2009 Comprehensive approach to modeling and simulation of photovoltaic arrays. *IEEE Trans. Power Electron.* 24(5): 1198–1208. https://doi.org/10.1109/TPEL.2009.201386
- Zhou X, Liu Q, Ma Y and Xie B 2021 DC-link voltage research of photovoltaic grid-connected inverter using improved active disturbance rejection control. *IEEE Access* 9: 9884–9894.
  - https://doi.org/10.1109/ACCESS.2021.305 0191